A Facile Approach to Fabricate Patterned Surfaces for Enhancing Light Efficiency of COB-LEDs

Xingjian Yu, Bin Xie, Bofeng Shang, Weicheng Shu, and Xiaobing Luo, *Senior Member, IEEE*

***Abstract*— Light efficiency of chip-on-board light-emitting diodes (COB-LEDs) is much lower than the single-chip packaging LEDs due to its flat phosphor layer, and hemispherical phosphor layer realization is a great challenge in COB-LEDs packaging due to the low surface tension of the phosphor gel. In this paper, we demonstrated a facile method to fabricate patterned surfaces to deal with this challenge. First, nanosilica (NS) particles with average diameter of 70 nm were fabricated by hydrolyzing the tetraethoxysilane and further modified by 1H,1H,2H,2H-perfluorooctyl-trichlorosilane, then patterned surfaces were fabricated by introducing a tailored template into the NS coating process. The results show that the NS coated surfaces display repellency to the water and phosphor gel with porous lotus leaf-like hierarchical structure, when the particle deposition density (PDD) of the NS particles increases from 0 to 6 g/m2, the contact angle (CA) of water increases from 34° to 161°, and the CA of phosphor gel increases from 22° to 145°. Hemispherical phosphor layer was achieved with the patterned surfaces when the PDD is 1.5 g/m2. Compared to the conventional flat phosphor layer, the hemispherical phosphor layer enhances the light efficiency by 11.74% and 14.52% for 4000 and 5000 K COB-LEDs.**

***Index Terms*— Chip-on-board light-emitting diodes (COB-LEDs), light efficiency, patterned surface.**

I. Introduction

OVER the past decades, light-emitting diodes (LEDs) have made remarkable progress in epitaxy growth, chip design, packaging materials and packaging technology, and have widely been applied in our daily lighting [1]. For industrial application, LEDs are manufactured into single-chip packaging module [2]–[4], as shown in Fig. 1(a) or integrated into chip-on-board packaging module (COB-LEDs) [5], as shown in Fig. 1(b), and the latter is becoming more and more popular due to its advantages of high luminous flux, compact size, and low cost [1]. However, compared to the single-chip packaging module, the COB-LEDs) suffers from lower light efficiency because of the total internal reflection (TIR) which happens at the flat encapsulant-air interface with an extremely small critical angle of 38°–45° [6]–[8], and the drop of the light efficiency would worsen the thermal reliability of LEDs [9]. Quite a few methods were proposed to eliminate the TIR including scattering layer [Fig. 1(c)] [6], [7] and patterned leadframe substrate [Fig. 1(d)] [8]. The principle of these methods is to redirect the light that reflected from the encapsulant-air interface to the angle within the critical angle, however, quite part of the reflected light is absorbed by the encapsulant due to the relatively long propagate path.

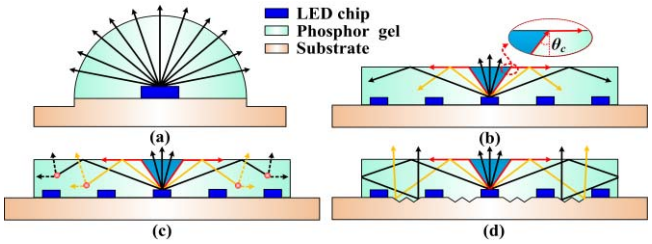

Fig. 1. (a) Single-chip packaging module. (b) TIR of COB packaging module. (c) COB packaging module with scattering layer. (d) COB packaging module with patterned leadframe substrate.

A more feasible method is to guide the light to emit out directly through roughened LED chip [10] and roughened [11], [12] or domed encapsulation layer [Fig. 1(a)] [5]. In general, the encapsulant would spread over flat surfaces with a contact angle (CA) smaller than 30° due to the low surface tension of encapsulant, therefore, to realize domed encapsulation layer on flat surface is a great challenge in LED packaging. In our previous study, we realized a cylindrical encapsulation layer for COB-LEDs to eliminate the TIR, the phosphor gel was coated onto the preheated LED substrate, and it was cured before spread to its final geometry due to the thermosetting property of the silicone [5]. However, the CA of the phosphor gel is smaller than 70°, and the theoretical optimized encapsulation layer is hemispherical with CA of 90°, therefore, more works need to be done.

In recent years, patterned surfaces contain both liquid-repellency surface and liquid-wetting surface were developed and proposed to have potential applications in liquid

Manuscript received May 19, 2017; revised July 4, 2017; accepted July 24, 2017. Date of publication August 14, 2017; date of current version September 20, 2017. This work was supported in part by the National Natural Science Foundation of China under Grant 51625601, Grant 51576078, and Grant 51606074, and in part by the Fundamental Research Funds for the Central Universities under Grant 2016JCTD112. The review of this paper was arranged by Editor J. Huang. *(Corresponding author: Xiaobing Luo.)*

The authors are with the School of Energy and Power Engineering, Huazhong University of Science and Technology, Wuhan 430074, China (e-mail: Luoxb@hust.edu.cn).

Color versions of one or more of the figures in this paper are available online at http://ieeexplore.ieee.org.

Digital Object Identifier 10.1109/TED.2017.2734105

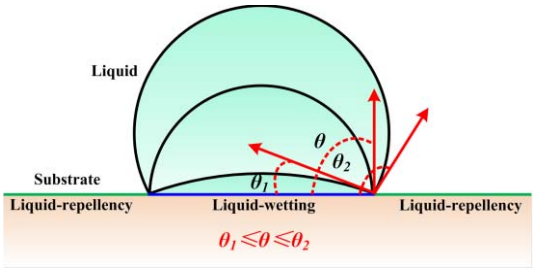

Fig. 2. Liquids self-assembly principle of patterned surfaces.

transport [13], [14], enhanced condensation [15], [16] boiling heat transfer [17], [18], and the directed growth of thin films [19]. Further, such surfaces can also serve as templates for the wettability-driven self-assembly of low surface tension liquids [20], which offer a solution to realize domed encapsulation layer. Fig. 2 shows the liquids self-assembly principle of patterned surfaces. Liquids on the patterned surfaces are restrained within the liquid-wetting surface, and the CA can be adapted to any value between θ_1 and θ_2. θ_1 is the CA between the liquids and the liquid-wetting surface, and θ_2 is the CA between the liquids and liquid-repellency surface. Compared to the homogeneous liquid-repellency or liquid-wetting surfaces, there are two main advantages of the patterned surfaces, one is the CA is adaptable, another is the wetting pattern of liquids can be precisely controlled.

For applying the patterned surfaces in LED packaging, the main challenge is to fabricate oleophobic surface with low cost. Compared to the hydrophobic surfaces which only display repellency to high surface tension liquids such as water (0.072 N/m), the fabrication of oleophobic surfaces display repellency to low surface tension liquids requires more advanced technology. To achieve such a surface property, surfaces should be modified with a combination of hierarchical surface structure and low surface energy functionality [21].

Hierarchically structured surfaces possess more than one scale roughness is an effective way to enlarge the apparent CA between liquid droplets and solid substrates by supporting the liquids in Cassie–Baxter state [22], and the low surface energy functionality of the surfaces is important for enlarge the intrinsic CA defined by Young's equation [23]. Over the past decades, various strategies have been proposed to generate oleophobic surfaces [24]–[26]. First, hierarchically structured surfaces are prepared by numerous methods including lithography [27], etching [28], electrospinning [29], electroless galvanic deposition [30], and anodization [31], then the hierarchically structured surfaces are generally functionalized with fluorinated alkylsilanes [32], [33]. However, most of the proposed approaches are still not cost effective in many applications due to the expensive and complex process of fabricating hierarchically structured surfaces. The random distribution of nanoparticles on surfaces can be an alternative and inexpensive method for the fabrication of hierarchical surface structures, the nanoscale texture is formed by the intrinsic size of nanoparticles, and the microscale texture is formed by aggregation of nanoparticles [34]–[38].

In this paper, we proposed a simple and inexpensive method to fabricate patterned surfaces. First, nanosilica (NS) particles with average diameter of 70 nm were fabricated by hydrolyzing the tetraethoxysilane (TEOS) and modified by 1H,1H,2H,2H-perfluorooctyltrichlorosilane (FOTS), the FOTS is chosen to modify the NS particles due to its low surface energy functional groups ($-CF_2$ and $-CF_3$) [21], [38]. Second, the FOTS-NS particles were deposited on silicon surface using spray coating method. By introducing a tailored template into the NS particles deposition process, patterned surfaces were achieved and applied in LED packaging to realize hemispherical phosphor layer geometry. The chemical compositions and morphology of the FOTS-NS particles were characterized. The wettability and morphology of the FOTS-NS coated surfaces were characterized. The light efficiency enhancement of the COB-LEDs with the patterned surfaces was demonstrated.

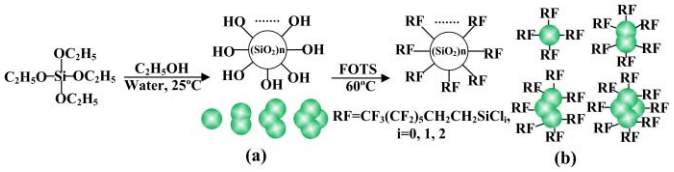

Fig. 3. FOTS-modified NS particles fabrication process. (a) NS particles preparation. (b) NS particles modification.

II. Methodology

A. Materials

TEOS (98%) was obtained from Alladdin and its molecular structure can be represented by the following formula: $Si(OC_2H_5)_4$. FOTS (99%) was purchased from Guidechem and its molecular structure can be represented by the following formula: $CF_3(CF_2)_5CH_2CH_2SiCl_3$. Ethanol (99.7%), ammonia (28%–30%), and acetone (99%) were used. Pure water and phosphor gel were used to characterize the wettability of the prepared surface. The phosphor gel was also used as the encapsulant material in LED packaging, it consists of phosphor (0.1 g, diameter of 13 μm, YAG-04, Intematix) and silicone (1 g, OE6550A/B, Dow corning), its surface tension was measured as 0.034 N/m, and its viscosity was measured as 4.2 Pa·s at 25 °C. The silicon substrates are provided by Dalian University of Technology.

B. Synthesis of FOTS-NS Particles

Fig. 3 shows the FOTS-NS particles fabrication process, it consists of two steps.

1) NS particles preparation. The NS particles were prepared according to the Stöber method [39]. First, ethanol (100 mL) and ammonia (7 mL) were mixed homogenously via stirring at 700 rpm for 15 min at 25 °C, then TEOS (8 mL) was added, after stirring for 48 h, pristine NS particles were obtained in the suspension.
2) NS particles modification. The pristine NS particles were separated by centrifugation and dispensed in acetone (100 mL) after washing with acetone three times, then the suspension was heated to 60 °C, adding the FOTS (8 mL) into the suspension and stirring at 700 rpm for 12 h. The resultant FOTS-NS particles were obtained

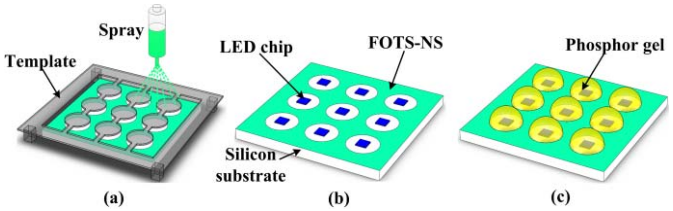

Fig. 4. Fabrication process of the patterned surfaces and its application in LED packaging. (a) Coating the FOTS-NS. (b) Bonding the LED chip. (c) Coating the phosphor gel.

by residual FOTS removal through four cycles of centrifugation/redispersion in acetone. Finally, the resultant product was dispersed in ethanol for surface coating.

C. Patterned Surfaces Preparation and Application for COB-LEDs Packaging

Fig. 4 shows the fabrication process of the patterned surfaces and its application in COB-LEDs packaging, it contains three steps: 1) cleaning the silicon substrate in acetone by bath sonication for 30 min and rinsed with deionized water for three times, then covering a tailored template on the substrate and spraying FOTS-NS on the uncovered surface at 20-cm distance using spray gun (VL-SET, Paasche Airbrush Company) at 300 kPa air pressure; 2) bonding the LED chip on the LED substrate; and 3) coating the phosphor gel onto the LED chip and substrate and curing it.

D. Characterization

The chemical composition of FOTS-NS particles were studied by X-ray photoelectron spectroscopy (XPS, AXIS-ULTRA DLD-600W, Kratos). The binding energies were referenced to 285 eV as determined by the locations of the maximum peaks on the C 1s spectra of the hydrocarbon associated with adventitious contamination, while the F 1s peak maximum was set at 689 eV. The morphology of the FOTS-NS particles was characterized with transmission electron microscope (TEM, Tecnai-G20, FEI).

The morphologies of the FOTS-NS coated surfaces were observed by scanning electron microscope (SEM, JSM-7600F, JEOL). The wettability of FOTS-NS coated surfaces for water and phosphor gel was determined by measuring static CA and CA hysteresis (CAH, difference between the advancing CA and receding CA) using the drop shape analyzer (DSA25, Kruss). The reported CA and CAH are the average of measurements obtained at three different points on each sample surface with liquid droplets (diameter of 2 mm). The water droplets bouncing phenomenon on the prepared surfaces were observed with high-speed camera (SA3 120K, Photron).

The light efficiency of LED modules was measured with an integrating sphere of 1 m in diameter (ATA-1000, Everfine).

III. Results and Discussion

A. Morphology and Chemical Characterization of the FOTS-NS Particles

Fig. 5(a) shows the TEM image of the FOTS-NS particles, it shows that the particles is closed to be a sphere with average diameter of 70 nm. Fig. 5(b)–(d) shows the transmittance test

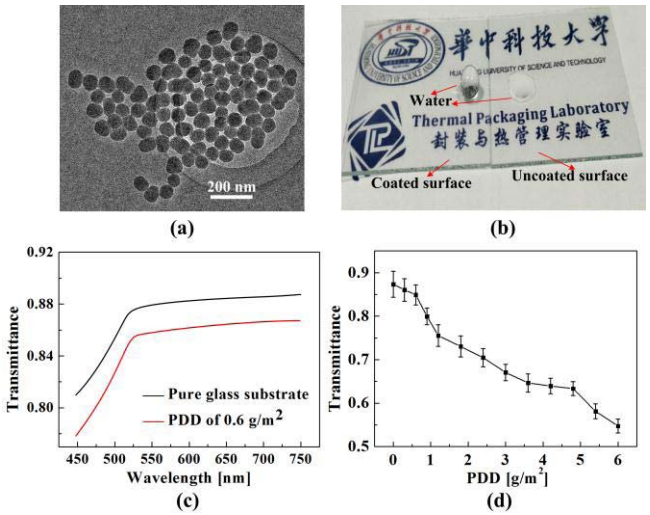

Fig. 5. FOTS-modified NS. (a) TEM imagine of the FOTS-NS particles. (b) Pure glass substrate and FOTS-NS coated substrate with PDD of 0.6 g/m^2. (c) Transmittance spectra of the two substrates shown in (b). (d) Transmittance of glass substrate with PDD from 0 to 6 g/m^2.

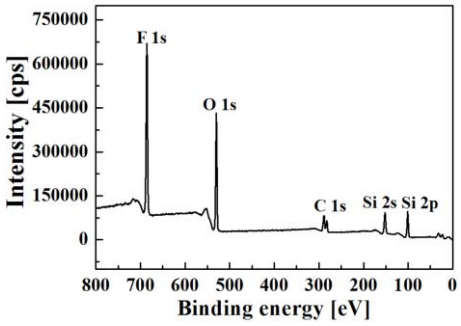

Fig. 6. XPS spectra of the FOTS-modified NS.

TABLE I
Atom Concentrations of the Detected Chemical Elements

Peak	F 1s	O 1s	C 1s	Cl 2p	Si 2p
Position BE (ev)	690	535	285	200	104
Atomic concentration (%)	33.53	28.53	21.00	0.01	16.94

results of the FOTS-NS particles. To test the transmittance, the particles were coated on a 0.5-mm-thick glass substrate with particle deposition density (PDD) from 0 to 6 g/m^2, the PDD is defined as the ratio of the NS particles deposition mass to the surface area. Fig. 5(b) shows the image of the pure and FOTS-NS coated (PDD of 0.6 g/m^2) glass substrates, Fig. 5(c) shows the transmittance spectra of the two substrates, it shows that the FOTS-NS coated glass substrate exhibits superhydrophobicity while keeps high transparency. Fig. 5(d) shows the transmittance of the FOTS-NS coated substrate with PDD from 0 to 6 g/m^2, it indicates that the transmittance decreases with the PDD.

Fig. 6 shows the XPS spectra of the FOTS-NS particles. Si 2p, C 1s, O 1s, F 1s peaks were detected at binding energy around 104, 285, 535, and 690 eV, respectively. Table I shows the atom concentrations of Si 2p, Cl 2p, C 1s, O 1s and F 1s. The atomic concentration ratio of F/C is 1.59 which indicates a strong surface enrichment of fluorine. Besides, the atomic

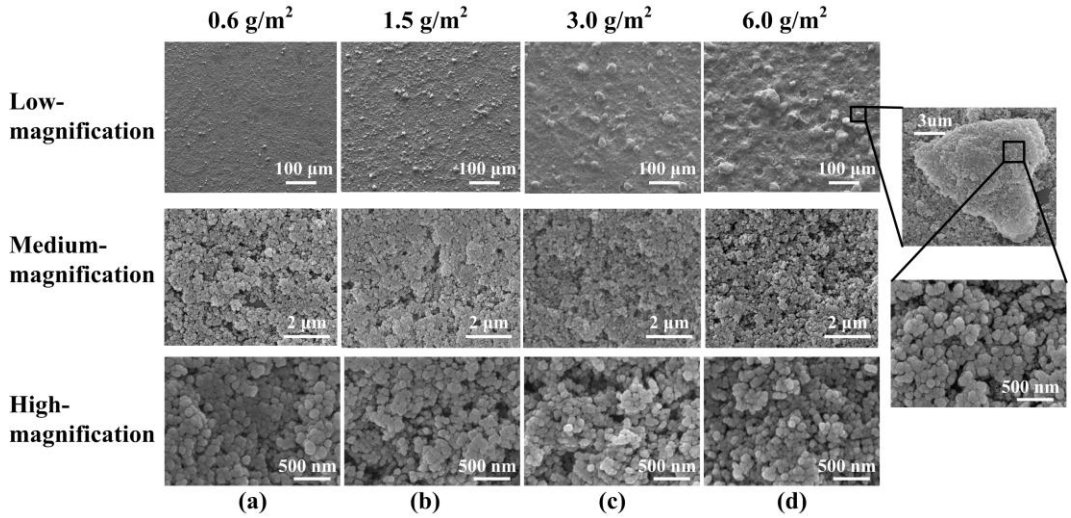

Fig. 7. Surface morphology of the FOTS-modified NS coated surfaces with various PDD. (a) 0.6 g/m^2. (b) 1.5 g/m^2. (c) 3 g/m^2. (d) 6 g/m^2.

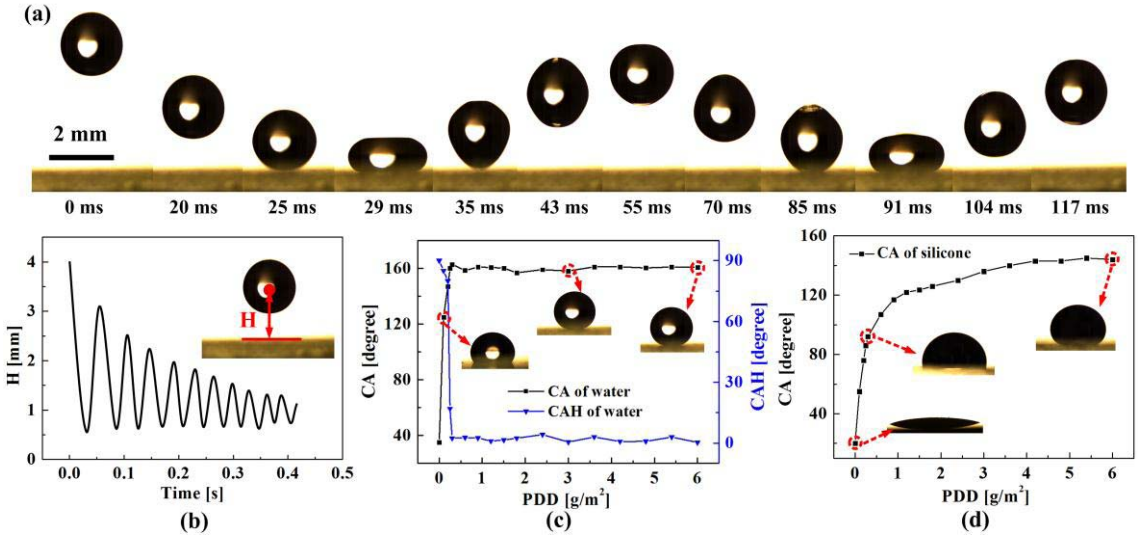

Fig. 8. Wettability characterization results of water and phosphor gel droplets on the FOTS-modified NS coated surfaces. (a) and (b) Bouncing phenomenon of water droplets (diameter of 2 mm) on the surface with PDD of 1.5 g/m^2. (c) CA and CAH of water droplets (diameter of 2 mm) on the surfaces with various PDD. (d) CA of phosphor gel droplets (diameter of 2 mm) on the surfaces with various PDD.

concentration of Cl 2p is only 0.01% which indicates that the FOTS were sufficient reacted with the hydroxy of the NS particles.

B. Surface Morphology and Wettability Characterization of the FOTS-NS Coated Surfaces

Fig. 7 provides the SEM images of the surfaces with PDD of 0.6, 1.5, 3, and 6 g/m^2, respectively. It can be found that the NS particles naturally generate porous lotus leaf-like hierarchical structure on the surfaces. The microscale texture is formed by the aggregation of the FOTS-NS particles, and the nanoscale texture is structured by the intrinsic size of the FOTS-NS particles. The main differences of the surfaces are lie on the microscale texture as shown in the low-magnification SEM images, while the nanoscale texture is similar as shown in the medium-and high-magnification SEM images. The average dimensions of microscale texture increases with PDD, besides, at low PDD, only protuberant microtexture was observed, while at high PDD, sunk microscale texture appears and increases with PDD.

Water and phosphor gel repellency of the FOTS-NS coated surfaces were characterized. The bouncing phenomenon of a water droplet (diameter of 2 mm) on the surface with PDD of 1.5 g/m^2 is shown in Fig. 8(a) and (b). Fig. 8(a) indicates that the water droplet bounces off the surface spontaneously after it impacts the surface. Fig. 8(b) shows the time evolution of the height of the droplet's barycenter to the surface, it shows that the water droplets can easily bouncing from the surface for many times, which indicates the surface is highly repellency to the water. Fig. 8(c) shows the measured CA and CAH of water droplets (diameter of 2 mm) on the surfaces with PDD varies from 0 to 6 g/m^2, it indicates that the surfaces display superhydrophobicity when the PDD lager than 0.3 g/m^2, the CA of the water reaches to 160° and the CAH is less than 4°. Fig. 8(d) shows the CA of phosphor gel droplet (diameter of 2 mm) on the surfaces with PDD varies from 0 to 6 g/m^2,

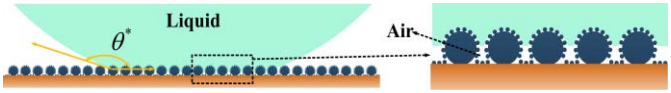

Fig. 9. Schematic of the Cassie–Baxter state.

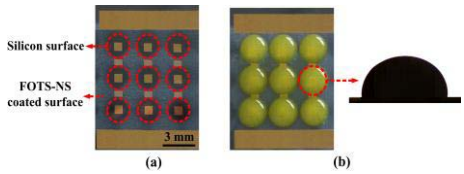

Fig. 10. (a) Patterned surface. (b) Hemispherical phosphor gel geometry.

it implies that CA of the phosphor gel is strongly dependent on the PDD, as the PDD increases from 0 to 6 g/m^2, the CA between the phosphor gel and surfaces increases from 22° to 145°. Besides, due to the high viscosity of the phosphor gel (4.2 Pa·s), no bouncing phenomenon was observed for the phosphor gel droplets.

The wetting of the water and phosphor gel droplets on the coated surfaces can be described by the Cassie–Baxter state shown as Fig. 9. Ascribe to the hierarchically texture formed by the FOTS-NS particles, the liquid does not completely wet the surface texture, and pockets of air remain trapped underneath the liquid droplet, the apparent CA θ^* of this state can be determined by the Cassie–Baxter equation [19], given as

$$\cos\theta^* = f_{\mathrm{sl}}\cos\theta_Y - f_{\mathrm{lv}} \tag{1}$$

$$f_{\mathrm{sl}} + f_{\mathrm{lv}} = 1 \tag{2}$$

where f_{sl} represents the area fraction of the solid-liquid interface, and f_{lv} represents the area fraction of the liquid-vapor interface. θ_Y is the intrinsic CA of the droplets on a flat surface defined by Young's equation [20]

$$\cos\theta_Y = \frac{\gamma_{\mathrm{sv}} - \gamma_{\mathrm{sl}}}{\gamma_{\mathrm{lv}}} \tag{3}$$

where γ_{sv}, γ_{sl}, and γ_{lv} refer to the surface tension of solid-vapor, solid-liquid, and liquid-vapor interfaces, respectively.

The surface tension of water (0.072 N/m) is much higher than that of the phosphor gel (0.034 N/m), so the intrinsic CA of water on a surface is higher than that of the phosphor gel according to the Young's equation. As a consequence, the water droplets display lager CA than the phosphor gel droplets on the coated surface with same PDD. Besides, as the PDD increase, the microscale texture becomes larger and more compact. According to the studies [30], [40], the larger and compact texture prevents the droplets from impregnating the surface. Therefore, the CA of the phosphor gel increases with PDD.

C. Patterned Surface for COB-LEDs Packaging

Fig. 10 shows the patterned substrate fabricated by FOTS-NS coating and the hemispherical phosphor layer realized by the patterned surface. The patterned surface consists of pure silicon surface and FOTS-NS coated surface with PDD of 1.5 g/m^2, as shown in Fig. 8(d), the CA of phosphor gel

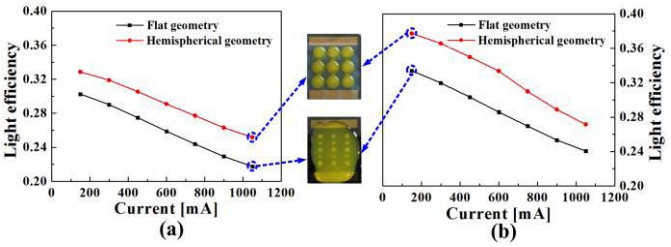

Fig. 11. Light efficiency comparison of LEDs with the flat and hemispherical geometries under various drive current. (a) CCT of 4000 K. (b) CCT of 5000 K.

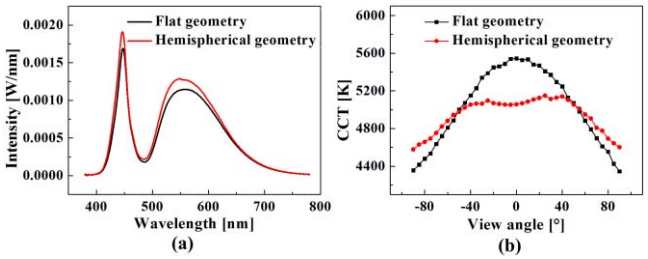

Fig. 12. Light spectra and CCT distributions of LEDs with flat and hemispherical phosphor geometries under CCT around 5000 K. (a) Light spectra. (b) CCT distribution.

on pure silicon surface is 22°, the CA of phosphor gel on FOTS-NS coated surface is 123°, so the CA of phosphor gel on the patterned surfaces can be adapted to a value between 22° and 123°. By controlling the coating volume of phosphor gel, it is very easy to realize hemispherical phosphor layer, as shown in Fig. 10(b).

After the phosphor gel been cured, the light efficiency of the LEDs was tested, LED modules with correlated color temperature (CCT) of 4000 and 5000 K were fabricated, and the conventional flat phosphor layer with same correlative color temperature was used to make comparison. Fig. 11 shows the light efficiency comparison of LEDs with the two geometries under drive current from 150 to 1050 mA at CCT of 4000 and 5000 K, it is calculated that a light efficiency enhancement of 11.74% and 14.5% was achieved. Such an enhancement is higher than the results reported in previous studies, (11.7% at 5000 K) [5], (12.24% at 5500 K) [6], and (9.7% at 3178 K) [12].

Fig. 12 shows the light spectra and CCT distributions of LEDs with flat and hemispherical phosphor geometries under CCT around 5000 K. Fig. 12(a) shows that the light spectra of LEDs with the two phosphor geometries is similar, and the peaks of the hemispherical geometry is higher than the flat geometry due to its higher efficiency. Fig. 12(b) shows that the hemispherical geometry have a more uniform CCT distribution, the CCT deviations of the flat and hemispherical geometry are 1200 and 572 K, respectively.

Reliability analysis of LEDs with the two phosphor geometries was conducted by online testing method [41], [42]. In the reliability experiments, LED samples were placed in an isothermal chamber with temperature of 120 °C. The light output of LEDs were collected and recorded in real time. Fig. 13 shows the normalized lumen maintenance of the two kinds of LEDs during the aging time of 180 h. It can be seen

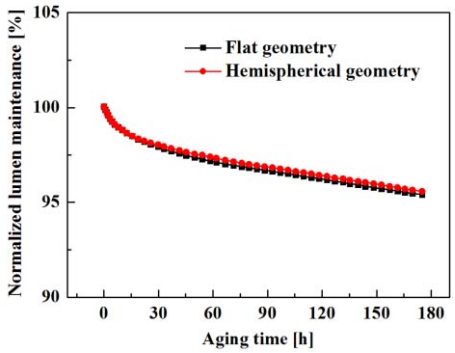

Fig. 13. Normalized lumen maintenance of the LEDs with flat and hemispherical geometry.

that both the two phosphor geometries exhibit high reliability and they show little difference. The lumen degradations of the flat and hemispherical geometries are calculated to be 4.59% and 4.42%, respectively.

IV. Conclusion

In summary, we have demonstrated a facile approach to fabricate patterned surfaces for enhancing light efficiency of COB-LEDs. FOTS-NS particles were fabricated and coated on silicon surface, by introducing a tailored template into the NS deposition process, patterned surfaces were achieved. The results show that the NS coated surfaces exhibit highly repellency to water droplets, and can realize high CA for phosphor gel with higher PDD. By setting the PDD of the NS coated surfaces of 1.5 g/m^2, hemispherical phosphor layer can be easily achieved. Compared to the conventional flat phosphor layer, the hemispherical phosphor layer enhances the light efficiency of COB-LEDs by 11.74% and 14.52% for 4000 and 5000 K, respectively.

Acknowledgment

The authors would like to thank Mr. Q. Teng for assistance with the SEM imaging, Mr. W. F. Tian for assistance with the TEM imaging, and Mr. Q. W. Huang for assistance with the XPS test.

References

[1] X. B. Luo, R. Hu, S. Liu, and K. Wang, "Heat and fluid flow in high-power LED packaging and applications," *Prog. Energy Combust. Sci.*, vol. 56, pp. 1–32, Sep. 2016.

[2] X. J. Yu, B. Xie, Q. Chen, Y. P. Ma, R. K. Wu, and X. B. Luo, "Thermal remote phosphor coating for phosphor-converted white-light-emitting diodes," *IEEE Trans. Compon., Packag., Manuf. Technol.*, vol. 5, no. 9, pp. 1253–1257, Sep. 2015.

[3] T. Cheng *et al.*, "Angular color uniformity enhancement of white LEDs by lens wetting phosphor coating," *IEEE Photon. Technol. Lett.*, vol. 28, no. 14, pp. 1589–1592, Jul. 15, 2016.

[4] H. C. Kuo *et al.*, "Patterned structure of remote phosphor for phosphor-converted white LEDs," *Opt. Exp.*, vol. 19, no. S4, pp. A930–A936, 2011.

[5] X. J. Yu, B. Xie, B. F. Shang, Q. Chen, and X. B. Luo, "A cylindrical tuber encapsulant geometry for enhancing optical performance of chip-on-board packaging light-emitting diodes," *IEEE Photon. J.*, vol. 8, no. 3, pp. 1–9, Jun. 2016.

[6] H. Zheng, L. Li, X. Lei, X. J. Yu, S. Liu, and X. B. Luo, "Optical performance enhancement for chip-on-board packaging LEDs by adding TiO_2/silicone encapsulation layer," *IEEE Electron Device Lett.*, vol. 35, no. 10, pp. 1046–1048, Oct. 2014.

[7] R. L. Liang, F. Wu, S. Wang, Q. Chen, J. N. Dai, and C. Q. Chen, "Enhanced optical and thermal performance of eutectic flip-chip ultraviolet light-emitting diodes via AlN-doped-silicone encapsulant," *IEEE Trans. Electron Devices*, vol. 64, no. 2, pp. 467–471, Feb. 2017.

[8] Z.-T. Li, Q.-H. Wang, Y. Tang, C. Li, X.-R. Ding, and Z.-H. He, "Light extraction improvement for LED COB devices by introducing a patterned leadframe substrate configuration," *IEEE Trans. Electron Devices*, vol. 60, no. 4, pp. 1397–1403, Apr. 2013.

[9] Y. P. Ma, R. Hu, X. J. Yu, W. C. Shu, and X. B. Luo, "A modified bidirectional thermal resistance model for junction and phosphor temperature estimation in phosphor-converted light-emitting diodes," *Int. J. Heat Mass Transf.*, vol. 106, pp. 1–6, Mar. 2017.

[10] Z. G. Zang, X. F. Zeng, J. H. Du, M. Wang, and X. S. Tang, "Femtosecond laser direct writing of microholes on roughened ZnO for output power enhancement of InGaN light-emitting diodes," *Opt. Lett.*, vol. 41, no. 15, pp. 3463–3466, 2016.

[11] D. Wu, K. Wang, and S. Liu, "Enhancement of light extraction efficiency of multi-chips light-emitting diode array packaging with various microstructure arrays," in *Proc. IEEE 61st Electron. Compon. Technol. Conf. (ECTC)*, Jul. 2011, pp. 242–245.

[12] C. F. Lai, J. S. Li, and C. W. Shen, "High-efficiency robust free-standing composited phosphor films with 2D and 3D nanostructures for high-power remote white LEDs," *ACS Appl. Mater. Interfaces*, vol. 9, no. 5, pp. 4851–4859, 2017.

[13] L. Zhai *et al.*, "Patterned superhydrophobic surfaces: Toward a synthetic mimic of the Namib desert beetle," *Nano Lett.*, vol. 6, no. 6, pp. 1213–1217, 2006.

[14] Y. Zheng *et al.*, "Directional water collection on wetted spider silk," *Nature*, vol. 463, no. 7281, pp. 640–643, 2010.

[15] K. K. Varanasi, M. Hsu, N. Bhate, W. Yang, and T. Deng, "Spatial control in the heterogeneous nucleation of water," *Appl. Phys. Lett.*, vol. 95, no. 9, pp. 7–10, 2009.

[16] N. A. Patankar, "Supernucleating surfaces for nucleate boiling and dropwise condensation heat transfer," *Soft Matter*, vol. 6, no. 8, pp. 1613–1620, 2010.

[17] A. R. Betz, J. Xu, H. Qiu, and D. Attinger, "Do surfaces with mixed hydrophilic and hydrophobic areas enhance pool boiling?" *Appl. Phys. Lett.*, vol. 97, no. 14, pp. 1–4, 2010.

[18] H. Jo, H. S. Ahn, S. Kang, and M. H. Kim, "A study of nucleate boiling heat transfer on hydrophilic, hydrophobic and heterogeneous wetting surfaces," *Int. J. Heat Mass Transf.*, vol. 54, nos. 25–26, pp. 5643–5652, 2011.

[19] T. Balgar, S. Franzka, E. Hasselbrink, and N. Hartmann, "Laser-assisted fabrication of submicron-structured hydrophilic/hydrophobic templates for the directed self-assembly of alkylsiloxane monolayers into confined domains," *Appl. Phys. A Mater. Sci. Process.*, vol. 82, no. 1, pp. 15–18, 2006.

[20] S. P. R. Kobaku, A. K. Kota, D. H. Lee, J. M. Mabry, and A. Tuteja, "Patterned superomniphobic-superomniphilic surfaces: Templates for site-selective self-assembly," *Angew. Chem.-Int. Ed.*, vol. 51, no. 40, pp. 10109–10113, 2012.

[21] A. K. Kota, G. Kwon, and A. Tuteja, "The design and applications of superomniphobic surfaces," *NPG Asia Mater.*, vol. 6, no. 7, p. e109, 2014.

[22] A. B. D. Cassie and S. Baxter, "Wettability of porous surfaces," *Trans. Faraday Soc.*, vol. 40, no. 5, pp. 546–551, 1944.

[23] T. Young, "An essay on the cohesion of fluids," *Philos. Trans. Roy. Soc. London*, vol. 95, no. 1, pp. 65–87, 1805.

[24] A. Tuteja *et al.*, "Designing superoleophobic surfaces," *Science*, vol. 318, no. 5856, pp. 1618–1622, 2007.

[25] G. Perry, Y. Coffinier, V. Thomy, and R. Boukherroub, "Sliding droplets on superomniphobic zinc oxide nanostructures," *Langmuir*, vol. 28, no. 1, pp. 389–395, 2012.

[26] T. C. Rangel, A. F. Michels, F. Horowitz, and D. E. Weibel, "Superomniphobic and easily repairable coatings on copper substrates based on simple immersion or spray processes," *Langmuir*, vol. 31, no. 11, pp. 3465–3472, 2015.

[27] H. J. Choi, S. Choo, J. H. Shin, K. I. Kim, and H. Lee, "Fabrication of superhydrophobic and oleophobic surfaces with overhang structure by reverse nanoimprint lithography," *J. Phys. Chem. C*, vol. 117, no. 46, pp. 24354–24359, 2013.

[28] L. Cao, T. P. Price, M. Weiss, and D. Gao, "Super water- and oil-repellent surfaces on intrinsically hydrophilic and oleophilic porous silicon films," *Langmuir*, vol. 24, no. 5, pp. 1640–1643, 2008.

[29] S. Pan, A. K. Kota, J. M. Mabry, and A. Tuteja, "Superomniphobic Surfaces for Effective Chemical Shielding," *J. Amer. Chem. Soc.*, vol. 135, no. 2, pp. 578–581, 2013.
[30] C. Yuan, M. Y. Huang, X. J. Yu, Y. P. Ma, and X. B. Luo, "A simple approach to fabricate the rose petal-like hierarchical surfaces for droplet transportation," *Appl. Surf. Sci.*, vol. 385, pp. 562–568, Nov. 2016.
[31] D. Wang, X. Wang, X. Liu, and F. Zhou, "Engineering a titanium surface with controllable oleophobicity and switchable oil adhesion," *J. Phys. Chem. C*, vol. 114, no. 21, pp. 9938–9944, 2010.
[32] P. Muthiah, B. Bhushan, K. Yun, and H. Kondo, "Dual-layered-coated mechanically-durable superomniphobic surfaces with anti-smudge properties," *J. Colloid Interface Sci.*, vol. 409, pp. 227–236, 2013.
[33] J. Y. Lee, S. Pechook, B. Pokroy, and J. S. Yeo, "Multilevel hierarchy of fluorinated wax on CuO nanowires for superoleophobic surfaces," *Langmuir*, vol. 30, no. 51, pp. 15568–15573, 2014.
[34] Y. Gao, Y. Huang, S. Feng, G. Gu, and F. L. Qing, "Novel superhydrophobic and highly oleophobic PFPE-modified silica nanocomposite," *J. Mater. Sci.*, vol. 45, no. 2, pp. 460–466, 2010.
[35] S. Nishizawa and S. Shiratori, "Water-based preparation of highly oleophobic thin films through aggregation of nanoparticles using layer-by-layer treatment," *Appl. Surf. Sci.*, vol. 263, pp. 8–13, Dec. 2012.
[36] H. Vahabi, W. Wang, S. Movafaghi, and A. K. Kota, "Free-standing, flexible, superomniphobic films," *ACS Appl. Mater. Interfaces*, vol. 8, no. 34, pp. 21962–21967, 2016.
[37] P. S. Brown and B. Bhushan, "Mechanically durable, superomniphobic coatings prepared by layer-by-layer technique for self-cleaning and anti-smudge," *J. Colloid Interface Sci.*, vol. 456, pp. 210–218, Oct. 2015.
[38] E. J. Park, D. H. Kim, J. H. Lee, S. Ha, C. Song, and Y. D. Kim, "Fabrication of a superhydrophobic and oleophobic PTFE membrane: An application to selective gas permeation," *Mater. Res. Bull.*, vol. 83, pp. 88–95, Nov. 2016.
[39] W. Stöber, A. Fink, and E. Bohn, "Controlled growth of monodisperse silica spheres in the micron size range," *J. Colloid Interface Sci.*, vol. 26, no. 1, pp. 62–69, 1968.
[40] B. Bhushan and E. K. Her, "Fabrication of superhydrophobic surfaces with high and low adhesion inspired from rose petal," *Langmuir*, vol. 26, no. 11, pp. 8207–8217, 2010.
[41] Q. Chen, Q. Chen, and X. B. Luo, "Note: An online testing method for lifetime projection of high power light-emitting diode under accelerated reliability test," *Rev. Sci. Instrum.*, vol. 85, no. 9, pp. 1–4, 2014.
[42] Q. Chen, Q. Chen, S. Liu, and X. B. Luo, "A design for *in-situ* measurement of optical degradation of high power light-emitting diodes under accelerated life test," *IEEE Trans. Device Mater. Rel.*, vol. 14, no. 2, pp. 645–650, Jun. 2014.

Authors' photographs and biographies not available at the time of publication.